

Coal Particle Flow Patterns for O₂ Enriched, Low NO_x Burners

Final Technical Report
Performance Period: 10/1/00 – 9/30/04

Prepared by

Jennifer Sinclair Curtis
School of Chemical Engineering
Purdue University
West Lafayette, IN 47907-2100

Report issued on August 1, 2005

Submitted to

AAD Document Control
MS 921-143
U.S. Department of Energy - NETL
P.O. Box 10940
Pittsburgh, PA 15236-0940

Under Contract DE-FG26-00NT40816

Disclaimer of Endorsement

This report was prepared as an account of work sponsored by an agency of the United States Government. Neither the United States Government nor any agency thereof, nor any of their employees, makes any warranty, expressed or implied, or assumes any legal liability or responsibility for the accuracy, completeness, or usefulness of any information, apparatus, product, or process disclosed, or represents that its use would not infringe privately owned rights. Reference herein to any specific commercial product, process, or service by trade name, trademark, manufacturer, or otherwise, does not necessarily constitute or imply its endorsement, recommendation, or favoring by the United States Government or any agency thereof. The views and opinions of authors expressed herein do not necessarily state or reflect those of the United States Government or any agency thereof.

EXECUTIVE SUMMARY

This project involved a systematic investigation examining the effect of near-flame burner aerodynamics on standoff distance and stability of turbulent diffusion flames and the resultant NO_x emissions from actual pulverized coal diffusion flames. Specifically, the scope of the project was to understand how changes in near-flame aerodynamics and transport air oxygen partial pressure can influence flame attachment and coal ignition, two properties essential to proper operation of low NO_x burners. Results from this investigation utilized a new 2M tall, 0.5m in diameter combustor designed to evaluate near-flame combustion aerodynamics in terms of transport air oxygen partial pressure (Po₂), coal fines content, primary fuel and secondary air velocities, and furnace wall temperature furnish insight into fundamental processes that occur during combustion of pulverized coal in practical systems. Complementary cold flow studies were conducted in a geometrically similar chamber to analyze the detailed motion of the gas and particles using laser Doppler velocimetry.

TABLE OF CONTENTS

	Page
Abstract	5
2M Furnace	6
Hot Flow Studies – Summary	8
Hot Flow Studies – Detailed Results	9
Wall Temperature Effects	10
Oxygen Partial Pressure Effects	11
Effect of Fines	13
LDV/PDPA System	14
Cold Flow Studies – Summary	16
Cold Flow Studies – Detailed Results	17
Effect of Velocity Ratio	18
Effect of Particle Size Distribution	19
Figures – Hot Flow Studies	23
Figures – Cold Flow Studies	32
Table	43
References	44
Articles and Presentations	45
Students Supported	46

ABSTRACT

This final technical report summarizes the key findings from our investigation into coal particle flow patterns in burners. Specifically, we focused on the effects of oxygen enrichment, the effect of fines, and the effect of the nozzle velocity ratio on the resulting flow patterns. In the cold flow studies, detailed measurements using laser Doppler velocimetry (LDV) were made to determine the details of the flow. In the hot flow studies, observations of flame stability and measurements of NO_x were made to determine the effects of the flow patterns on burner operation.

HOT FLOW STUDY

The 2M Furnace

A novel 2 meter tall furnace (Figures 1 and 2) was designed and constructed for conducting the hot flow studies. This furnace is designated the “2M” furnace. The new 2M furnace was specifically built to evaluate combustion phenomena in the near-flame region. Hence, furnace operation, control methodology and sampling focused on the near-flame region. In this instance, wall effects were considered to be potential impingement of the flame or gas jets on the furnace walls. Jets typically exert a 9-10° angle of divergence, which was used to determine the minimum furnace diameter (18”) to prevent wall impingement. The total furnace length of the 2M furnace was 6 ft (2 m) to allow for burnout and minimize exhaust effects on the flow characteristics within the hot reactive section.

With a furnace diameter of 0.5m, it was determined that the heat of combustion from a 20kW burner could not maintain sufficiently high wall temperatures to sustain combustion. Thus, the furnace design had to include external heating, and electric heaters embedded in the furnace walls were employed. The furnace walls were constructed of insulating refractory board made from compressed alumina oxide fibers.

The furnace configuration allowed for symmetrical construction and provided easy access for the observation and sampling ports. The octagonal design maintained radial symmetry and provided flat surfaces for mounting plate heaters. The furnace was constructed of 2 layers of 1” thick refractory board (Fibercraft 2300BRD, Thermcraft) surrounded by 4 inches of 8 pound Kaowool blanket insulation. The walls of the hot section were embedded in a 2” thick base made from the refractory board. The top of the furnace was constructed from a single 2” thick refractory board that fit tightly onto the hot section walls. The cool section was pressed into the base of the hot section and was supported by a stainless steel ashtrap. The use of the rigid insulation board with its extremely small thermal expansion coefficient and the sliding stainless steel plates

minimized the potential for leaks due to thermal cycling. The furnace walls were coated (QF-180 coating cement, Thermcraft) to prevent decomposition and minimize leakage into or out of the furnace. Exterior seams were taped and sealed with high temperature ceramic fabric dipped in the QF-180 cement. The cool section was lined with a Nextel 312 fabric skirt (3M) to prevent molten ash from collecting on the walls and causing damage upon removal. Moldable Inswool caulk was used to seal the seams between each section.

In addition to four stationary ports a translating sampling stage ran the full length of the hot section and was located at a right angle to the stationary ports and directly opposite the optical window described below. The combustion gases exit the furnace through a water-cooled 2" exhaust duct which conveys the gases to a centrifugal exhaust fan/cyclone (AGET 5N20-D1, AMET) where the majority of particulate matter entrained in the exhaust stream was removed. The cyclone was sized to remove 95 to 99 % of particles greater than 20 microns and 60% greater than 7 microns. Thus the system removed virtually all of the unburned coal and the majority of flyash not collected by the ash trap. The exhaust included a dilution air system in addition to the water-cooled jackets to further cool the exhaust gases before entering the cyclone.

As the experimental analysis included evaluation of the near-flame region, it was desirable to include a full-length observation port in the furnace. This allowed researchers to conduct flow visualization studies, flame shape and length analyses without being limited by the field of view of conventional sampling ports. The flow visualization window was initially constructed of three sections of quartz 1/8" inch thick. The quartz sections were fitted into channels cut into the furnace walls and cemented in-place using moldable Kaowool caulking. The gaps between the quartz sections were also sealed with moldable Kaowool. A single quartz pane was later installed in a modified frame to increase maintainability and reduce inleakage. The quartz pane was sealed between multiple layers of Fibrefrax and pressed against the walls of the visualization port by means of a rigid angle-iron frame attached to the furnace superstructure. The

optical window section was also fitted with an access port to allow insertion of a compressed air wand for blowing soot off the window between runs.

Hot Flow Studies Results - Summary

In the 2M furnace, a combustion ratio greater than 1 was required for stable operation, where the combustion ratio is defined as the ratio of the combustion air velocity (V_c) to primary jet velocity (V_t). Increasing this ratio increases flame stability and promotes flame attachment. Increasing PO_2 and/or fines fraction in the pulverized coal also enhances combustion stability producing attached flames that were otherwise detached. NO_x emissions are reduced by up to 50% through flame attachment. The degree of oxygen enrichment necessary to produce attached flames decreased with increasing wall temperature. For always-attached flames, increasing PO_2 and the fraction of fines had little impact on total NO emissions. NO emissions increased with increasing combustion ratio for always-attached flames due to increased mixing between the primary fuel and combustion air jets, thereby increasing the local oxygen content.

Increasing fines content and velocity ratio reduced flame standoff distances for always-detached flames and produced stable detached flames that were otherwise unstable. However, neither fines nor transport air oxygen partial pressure greatly affected total NO emissions from always-detached flames. Increasing the velocity ratio did reduce total NO emissions for always-detached flames through reduced flame detachment and resultant premixing in the near-burner region.

For always-attached flames, increasing the combustion ratio stretches the flame producing a narrowed flame neck approximately 2 primary jet diameters below the burner. Decreasing the transport air oxygen partial pressure to 17% caused the narrowed flame neck to destabilize forming intermittent flamelets. Further reducing PO_2 to 12% produced a stable dual flame. The dual flame consisted of a short flame attached to the burner and a long detached flame with a flame front 18" below the burner. Observations of similar dual flames have not been found in published literature. The dual flame can be compared to staged combustion where one creates a primary fuel rich combustion zone

followed by a second combustion zone for burnout, however supplemental OFA is not required with the dual flame.

HOT FLOW STUDIES – Detailed Results

A major focus of the research was to conduct a *systematic* investigation of the effect of transport air oxygen partial pressure on coal combustion. Four transport air stream oxygen concentrations were initially targeted: 13%, 17%, 21% and 24%. These concentrations correspond to oxygen enrichment values of –100%, -30%, 0% and +15%, respectively (see Figure 3). Given the desired oxygen concentrations, an experimental test matrix was developed. The matrix is presented in Table 1. The experiments were conducted at a constant firing rate of 2 kg/hr, 725K (450°C) air preheat temperature, and overall stoichiometric ratio of 1.2. Experimental variables evaluated during the study in addition to oxygen concentration were primary jet velocity and initial wall temperature. During the experimental runs, a single variable was varied (i.e. oxygen partial pressure or wall temperature) while keeping the other variables constant. The stoichiometric ratio and the split between the primary (transport) air and secondary (combustion) air was varied slightly to maintain constant velocities for the various scenarios. The velocities of the primary jets did not differ by more than 3% and the annular velocities differed by less than 4%.

In the experiments, the 2M furnace walls were preheated to the initial set point temperature, operating flow rates and air preheat temperatures were set, and the furnace was lit. After the natural gas used for initial flame stabilization was turned off, flame stability was evaluated by observing the location of the flame front. Specific emissions that were measured included carbon dioxide, carbon monoxide, oxygen and nitrogen oxides as NO. Stable attached flames were considered to have flame fronts approximately $\frac{1}{4}$ to $\frac{1}{2}$ " below the nozzle. Flame standoff distances from the burner to the flame front were measured with of a yardstick mounted beside the flow visualization window. A stable combustion experiment lasted approximately 15 to 20 minutes.

The parametric study evaluated the effects of partial pressure of oxygen in the transport air stream on flame stability and NO_x emissions. The study included both visual observations of flame detachment and emissions analyses. A stable attached coal flame is presented in Figure 4. Figure 5 presents a stable detached coal flame. The flame front shown in Figure 5a is approximately 15 inches below the burner nozzle. The coal jet upstream of the flame front is shown in Figure 5b.

Wall Temperature Effects

The exhaust NO_x concentration data from the initial trials, adjusted to stoichiometric air conditions are plotted against average wall temperature in Figures 6 through 8 for the 17%, 21% and 24% transport air oxygen cases, respectively. [Note: The error bars in Figures 6 through 11 represent uncertainty in $\text{NO}_{x,\text{SR}}$ based on a propagation of error analysis on the NO_x emissions values (discussed in detail in Appendix C of Ogden's PhD thesis)]. These data are for attached flame conditions. The 12% transport air oxygen case did not produce a stable attached flame. During the initial trials, the furnace temperature slowly increased due to the heat of combustion. This temperature increase was most noticeable for a wall set point temperatures of 1020K (750°C). NO_x emissions also increased during the experiments. It was hypothesized that the increase in NO_x was due to the increased wall temperatures, thus concentration data gathered during individual runs are plotted as a function of wall temperature. Note that data from multiple experiments are presented. $\text{NO}_{x,\text{SR}}$ increases linearly with wall temperature for each partial pressure case at temperatures up to approximately 1220 K (950°C). The open symbols in Figures 6 through 8 represent data obtained for a combustion air to transport air velocity ratio of 3. The closed symbols are velocity ratio equal to 1.5. The velocity ratio gives a measure of the mixing intensity between the central and annular jets.

No stable detached flames were observed at wall set point temperatures of 1020K (750°C). Attached flames that detached during a run became unstable and blew out at these low temperatures. Higher furnace wall temperatures 1170K (900°C) supported

stable detached flames. Figure 9 presents $\text{NO}_{x,\text{SR}}$ as a function of wall temperature for both attached and detached flames. The detached flame data are denoted by open symbols and by a “D” in the legend. The data presented in Figure 9 for detached flames show a marked increase in overall NO_x emissions as compared with the attached flames. The NO_x emissions for the 17% oxygen detached flames are up to 33% higher than attached flames operating at the same conditions. This increase in NO_x emissions can be attributed to the increased mixing between the combustion air and the fuel prior to ignition. Under these conditions, fuel-nitrogen compounds volatilize under oxygen-rich conditions thereby promoting NO_x formation via Fuel NO_x mechanisms. Thermal (Zeldovich) and Prompt (Fenimore) NO_x reaction pathways are not considered to be major contributors of NO_x due to their long formation timescales at temperatures encountered in the pulverized coal furnace (Smart, 1992).

Oxygen Partial Pressure Effects

Increasing the partial pressure of oxygen in the transport air enhances combustion. This is shown by comparing Figures 6 through 8. As mentioned above, the 12% oxygen stream did not produce a stable attached flame. At 17% oxygen (Figure 6), stable attached flames were obtained at either 1020K or 1170K (750 or 900°C) wall temperature set points only for a velocity ratio equal to 3. Increasing the transport air to 21% oxygen produced stable attached flames at the higher wall temperature set point for the lower velocity ratio (1.5) scenarios. Further increasing the oxygen concentration to 24% produced stable attached flames for both velocity ratios at both wall temperature settings. These results are similar to the results of Spinti et al. (1997), which showed that reducing the primary oxygen concentration has a destabilizing effect on flame stability for co-fired combustion systems.

The attached flame data for all three oxygen partial pressure scenarios (17, 21 and 24%) are combined in Figure 10. The data in Figure 10 include both multiple experiments as well as temperature dependent data from individual experiments. The data in Figure 10 indicate that the concentration of oxygen in the transport air stream has little effect on the

overall NO_x emissions for attached flames. These findings are in agreement with Spinti et al. who found that reducing the primary oxygen from 21% to 13% had a minimal effect on NO production. However as noted above, increasing partial pressure of oxygen enhances combustion through increased flame stability.

The partial pressure of oxygen in the transport air stream also has little effect on NO_x emissions for the detached flames observed during the initial trials as shown in Figure 9. This was expected, as the flame fronts for the detached flames were 14 to 16" from the burner. This is well beyond the 7.5 to 8 duct diameters required for complete mixing of concentric jets (Thring & Newby, 1952, Becker et al., 1963). And, because the transport air makes up such a small fraction of the total combustion air (5 to 13.5%), the resulting impact of oxygen enrichment of the transport air stream is minimal. For example, the average oxygen concentration of the combined transport and combustion air streams ranges from 20.4% to 21.3% for the 12% and 24% transport air oxygen scenarios, respectively. However, oxygen partial pressure does affect flame detachment. Therefore oxygen enrichment can reduce overall NO_x emissions. Comparing emissions for the attached 24% oxygen flame at 1216K with the detached 12% flame at 1217K, one sees a 45% reduction in $\text{NO}_{x,\text{SR}}$ (207 vs. 317 ppm). Comparing emissions for an attached 21% oxygen case with those from a detached 17% oxygen case, each at approximately 1250K also shows a 45% reduction. These reductions are not through modifications in NO reaction pathways, but by enhancement of the overall combustion chemistry. The enriched oxygen cases exhibited better flame stability, which promotes combustion. This reduces the total amount of oxygen available for NO_x formation, thereby reducing overall pollutant emissions. Flame attachment also prevents air-fuel premixing causing the fuel nitrogen species to volatilize under fuel-rich conditions, which favors reduction to N_2 over oxidation to NO. Pershing (1976) observed similar dramatic reductions in NO_x when operating in attached (flame mode) vs. detached (reactor mode) conditions. When firing a high volatile bituminous coal, he observed 54% reductions in NO emissions for attached vs. detached flames.

Effect of Fines

A series of experiments was conducted to evaluate the impact of coal fines content on flame stability and NO_x emissions. For these studies, fines were considered to have particle diameters less than 10 microns. The experiments evaluated a no-fines coal where the fines had been removed, the base coal and a fines-enriched coal where the fines content had been increased through blending the base coal with fines. In summary, the fines experiments revealed that increasing the fraction of fines in pulverized coal:

- Produced stable attached flames that were otherwise detached, reducing NO_x emissions by up to 50% (see Figure 11). Emissions were reduced through flame attachment by creation of a fuel-rich flame zone where nitrogen volatiles were reduced to N₂.
- Reduced flame standoff distances for always-detached flames and stable detached flames that were otherwise unstable through increased reactivity, heat up times and volatility of the fines.
- Had little impact on resultant NO emissions in always-attached flames and always-detached flames. For attached flames, increasing fines did not appear to greatly increase early ignition or air/fuel mixing necessary to further reduce the oxygen content in the fuel rich central core. In detached flames, flame standoff distances were long enough for complete mixing of fuel and combustion air prior to ignition, thus negating any impact of fines enrichment on combustion stoichiometry.
- Negatively impacted fuel handling characteristics due to increased tendency to compact and form clumps.

COLD FLOW STUDY

LDV/PDPA System

A jet flow facility was designed in order to study the effects of particle size distribution, particle size, and fluid aerodynamics in the gas-solid flow. A schematic of the flow system is displayed in Figure 12

Figure 12 shows that the supplied air from the shop compressor is sent into two different lines. Airflow in the first line goes to the annular nozzle and loaded with tracing particles for the gas-phase velocity measurements. The tracing particles (glass beads less than 5 microns in diameter) are introduced into the flow by using a reverse cyclone. This line is open when an experimental study with a coaxial jet is performed. Airflow in the second line goes to the central nozzle and loaded with particles stored in two hoppers. The two hoppers shown in Figure 12 are employed to store two different sized particles used for the experimental study with bidisperse mixtures and are operated in parallel. This configuration allows for independent control of the particle feeding for the two different particle sizes in the binary mixture. When the gas-solid flows with monodisperse mixture are investigated, only one hopper is required and the air supply to the second hopper is stopped. The hopper used to store the fine particles (particle diameter less than 50 micron) is equipped with a screw feeder. The rotation speed of the screw feeder can be varied between 0 and 100 rpm and the mass flow rate of the fine particles increases with increasing the rotation speed. A screw feeder is needed to breakup the interaction between the fine particles in the hopper and to stabilize the flow of the fine particles from the hopper. On the other hand, when the hopper is filled with large particles with mean diameter greater than 50-micron, the screw feeder is not needed to stabilize the flow of particles. The flow rate of the larger particles depends mostly on the valve opening at the bottom of the hopper. A larger valve opening leads to an increase in the mass flow rate of these particles from the hopper. Particles from the storage hoppers are mixed with the air by means of a ventury eductor. The airflow is also seeded with tracing particles in order to measure the velocity characteristics of the gas-phase.

A copper pipe with a length-to-diameter ratio of 100 is used as the central jet nozzle. The large length-to-diameter ratio was used to ensure that fully developed turbulent pipe flow is achieved at the nozzle exit. The inner diameter of the central pipe, d , and the annular nozzle, D , are 0.56 inch and 1.254 inches, respectively. Flow straightener in the form of perforated plate is inserted in the annular nozzle in order to eliminate the angular velocity in the annular flow. The central and annular jets expand into an 18-inch x 18-inch test chamber to mimic the dimensions of the hot flow studies. The wall of the test chamber was made of non-absorbent optical grade pyrex glass. Fans are located in the collection area at the bottom of the test chamber and used to create a favorable pressure drop that assists the particles in exiting the test chamber. The fans entrain air from the surrounding with a maximum velocity of 0.06 m/s. In order to prevent any recirculation effect arising from the fans; a coarse dumping grid is installed and placed at the bottom of the test chamber just above the fans. The particles are collected in a container that sits on a load cell that is used to measure the mass of particles. The solid loading is calculated from this measurement and is monitored during experiments.

A two component of LDV/PDA was used to make measurement of the gas and particle-phase velocities as well as the particle size for different particles used in this investigation and developed by Aerometrics, Inc. A 5-W argon laser, which generates green and blue laser beams with wavelengths of 488 and 514 nm, respectively is used as the light source. The transmitting optics is the conventional dual beam LDV optics, which in this case, uses two Bragg Cells for to create a 40 MHz frequency shift for each colored beam in order to avoid directional ambiguity. There are two pairs of laser beams, green and blue beams coming out of the transmitting optics. The bisector of the green laser beams is parallel to the x-z plane and these beams are used to measure velocity component in the x direction. For the blue beams, the bisector of these beams is parallel to the y-z plane and these beams are used to measure the velocity component in the y direction. The receiving optics is oriented at an off-axis angle and it consists of a collection of lens, which produces a parallel beam of scattered light. This parallel beam is focused to vertical slit located behind the back lens. The vertical slit defines the effective length of probe volume from the where the scattered light could be received. For the current system, the

effective length of probe volume is 100 microns. Three photodetectors are used in the current system in order to extend the measurable particle size range while maintaining the resolution of the measurement. The scattered light energy is transformed into an electrical current by using a photomultiplier (PMT) and then, it is processed by using Aerometrics real time signal analyzer. The LDV/PDA system in the present study is placed on a traversing system with accuracy to within 10^{-4} inch.

In the present study, the measurements in gas-solid flows were made in two parts. The first part involved making measurement of the gas velocities in the presence of particles. The HV and burst threshold for detecting the tracing particles were set at 400 V and 0.05 mV, respectively. The second part involves making velocity measurement of particles. For the present system, two different particle sizes, 25-micron and 70-micron glass beads were used in the experiment. For the 25-micron particles, the HV and burst thresholds were set to 300 V and 0.2 mV, respectively. And for the 70-micron particles, the HV and burst threshold were set to 250 V and 0.5 mV, respectively. Higher values for HV and burst threshold are needed to make measurement for the larger particles. Moreover, the data rate in the present measurements varied between 1000 Hz near the centerline and 10 Hz near the edge of the flow. The percent coincidence ranged between 40-70% for the particles.

Cold Flow Study Results - Summary

Laser Doppler velocimetry and phase Doppler anemometry were also used to probe the detail motion of particles and gas in particle-laden jets. The first goal was to investigate the effect of velocity ratio on particle dispersion in coaxial particle-laden jets. The second goal was to explore the effect of particle size distribution on the motion of particles in particle-laden flows loaded with binary mixtures of two different sized particles.

The study was performed for three velocity ratios, $VR = 0, 1.0$, and 1.5 , and for two different sized particles: 25-micron and 70-micron glass beads with a solids loading of

0.5. LDV measurements show that the distribution of particles across the jet becomes more uniform with decreasing particle size for the same velocity ratio. Moreover, for the same particle size, the distribution of particles across the jet becomes more uniform as the velocity ratio increases. Flow visualization revealed that as the velocity ratio increases, the instantaneous particle structure tends to become wavier and less asymmetric. It was also observed that for $VR = 1.5$ the radial dispersions for both particles sizes are significantly enhanced.

An investigation with binary mixtures of 25-micron and 70-micron particles in downward pipe flow demonstrated that the addition of finer particles leads to an increase in the mean velocity of the coarse particles near the pipe. Moreover, the presence of the fine particles also enhances the velocity fluctuations of the coarse particles. The presence of coarse particles, however, does not affect the motion of the fine particles. Measurements of gas-phase velocity in the binary mixtures were also performed as a function of the mass fraction of the fine particles. Result from these measurements show that for the same total loading the dampening in the gas turbulence for the binary mixture consisting of 50% fines is less pronounced than a monodisperse suspension of coarse particles.

Results from this study also indicate that an increasing mass fraction of the finer particles in the mixture leads to a decrease in the radial mean velocity for the coarse particles. This effect is due to an increase in the resistance for the coarse particles to move in the flow as the number of fine particles is increased. Moreover, the ratio of the radial to axial mean velocity for the coarse particles decreases with increasing mass fraction of fine particles, implying a reduction in the radial dispersion of the coarse particles.

Cold Flow Studies – Detailed Results

Two types of particles were used in the cold flow studies, 25-micron and 70-micron glass beads with a density of $2,500 \text{ kg/m}^3$. The 70 micron particles are largely unresponsive to the gas flow field with $St > 5$; the 25 micron particles are partially responsive to the gas

flow field with St on the order of one. The particles are loaded at the central pipe and the particle mass loading is maintained at 0.5 for all velocity ratios. LDV/PDPA was used to measure time-averaged quantities such as mean velocities, rms velocities, and Reynolds stress. Flow visualization was used to observe instantaneous particle structures as a function of velocity ratio.

Effect of Velocity Ratio

The LDV data in Figures 13 and 14 showed that (in these figures VR represents velocity ratio and p and g represent particle and gas velocity measurements, respectively):

- An increase in the particle-phase axial velocity fluctuation along the jet centerline, after the initial decay, is generated via
 - The gradient of the particle mean velocity (the fan spreading mechanism). This mechanism is dominant for the 70 micron particles.
 - Response to the gas turbulent motion. This mechanism is dominant for the 25 micron particles.
- The 70 micron particles are largely unresponsive to the gas phase. Only at the highest velocity ratio do the 70 micron particles exhibit an increase in their velocity fluctuations downstream from the nozzle.
- The 25 micron particles are fairly responsive to the gas phase velocity fluctuations at all velocity ratios. The highest velocity ratio investigated showed the largest increase in the particle velocity fluctuations.

(In figures 13 and 14 the velocities that are reported are mean rms velocities based on at least 1000 single measurements. A histogram of the velocity deviations exhibits a Gaussian distribution whose standard deviation varied for each set of conditions. Yanta and Smith (1978) have shown that for a population size of 1000, the random error in rms velocities is approximately 4%.)

The flow visualization studies showed that (see Figures 15 through 20)

- Particles with Stokes numbers (St) on the order of one in a round laden jet tend to accumulate in a region of low vorticity, creating the “pine-tree” like structure. (Note:

The Stokes number is a key parameter in characterizing the interaction between particles and turbulent structures. St is defined as the ratio of the particle response time, t_p , to the eddy's time scale, t_e . The eddy's time scale is defined from the global length and velocity scales of the vortical structures. The length scale of these structures is on the order of the half jet width, L , and its velocity is approximated to be half of the maximum gas velocity, $U_{g,max}$.)

- The 70-micron particles with $St > 5$ tend to flow in straight-line trajectories in the coaxial jet as they exit from the nozzle. Velocity ratio has a very limited influence on the particle trajectories.
- For the 25-micron particles with $St < 5$, the instantaneous particle structures in the coaxial laden jet depend on velocity ratio and tend to become less symmetric with increasing velocity ratio.

Effect of Particle Size Distribution

In these studies, controlled bimodal mixtures of the two particle sizes (25 and 70 micron particles) were formed. The flow behavior of these particle mixtures were then analyzed using LDV. Single-phase measurements were also conducted at a $Re=8400$ using the glass bead tracing particles. The results analyzing the effect of particle size distribution are shown in Figures 21 to 27.

Figure 21 presents experimental measurements of the axial mean gas velocity, U_g , as a function of the mass fraction of the fine particles in the bidisperse suspension. There is no consistent trend in U_g with increasing the mass fraction of the fine particles. The magnitude of U_g for the 50% fine suspension is slightly higher than that of the 100% fine suspension.

The LDV measurements of the axial and radial components of the gas rms velocity, u_g' and v_g' , in the bidisperse suspensions with different fine mass fraction are displayed in Fig. 22. Increasing the mass fraction of the fine particles has a little effect on v_g' . Unlike v_g' , experimental results for u_g' show the dampening of u_g' is affected by PSD. The magnitude of u_g' in the 50%-fine system is not in the range between the 0% and 100%-

fine system, but it is surprisingly a little higher than the 0%-fine system. It is likely that the flattening in the U_g profile observed for the 0%-fine suspension induce a more pronounced dampening of u_g' than the presence of the fine particles in the 50%-fine suspension.

The radial profile of axial mean velocity for the 25-micron particles, U_f , in the bidisperse suspension is displayed in Fig. 23. Radial profiles of the mean velocity for the 70-micron particles, U_c , in the bidisperse suspension are shown in Fig. 24. The experimental measurements show an increase of approximately 10% in the magnitude of U_c near the pipe center and the radial profiles of U_c becomes less flat upon the addition of the finer particles. This increase is unlikely attributed to the decrease of the number of coarse particle (solid loading) when the mass fraction of fine particles is raised since the magnitude of U_c is not affected by solid loading for $m \leq 1.0$. In addition, measurements of the gas-phase axial mean velocity in the monodisperse suspension of coarse particles suggest that the modulation of gas-phase axial mean velocity with the addition of the fine particles will not be able to induce a 10% increase of U_c in the bidisperse suspension. This lead us to conclude that the 10% increase of U_c in the bidisperse suspension is mainly attributed to the presence of the fine particles. Since direct collision between two different sized particles is very unlikely, the author hypothesized that it is possible that the presence of the fine particles modifies the interaction between the gas and the coarse particles as if the apparent gas-phase viscosity is increased. One possible mechanism for the increase in the effective viscosity and hence, drag force is via an increase in the local velocity gradient, $\partial U_g / \partial r$ promoted by the fine particles, which move faster than the coarse particles. An increase in the gas-phase effective viscosity will lead to an increase in the momentum transfer rate via the interface drag force. One possible mechanism for the increase in the effective viscosity and hence, drag force is via an increase in the local velocity gradient, $\partial U_g / \partial r$ promoted by the presence of the fine particles which move faster than the coarse particles. This indicates that the fine particles are able to transfer part of their momentum to the coarse particles via the gas medium when the fine particles move faster than the coarse particles. Another intriguing question that may arise from the increased viscosity hypothesis is the modification in the wall-particle collisional

frequency by the increased apparent gas-phase viscosity. There is another possibility that the wall collision frequency is reduced as the fine particles put more resistance on the motion of the coarse particles. The reduction in wall frequency will reduce the momentum loss of the coarse particles and increase the magnitude of U_c .

Measurements of the axial rms velocities for the 70-micron particle, u_c' , as a function of mass fraction of the 25-micron particles are displayed in Fig. 25. The experimental results show that the axial rms velocity, u_c' shows a consistent increase in the magnitude as the finer particle mass fraction is raised. The increase in the magnitude of u_c' is partly attributed to the decrease in the number or solid loading of the 70-micron particles in the bidisperse suspension when the mass fraction of the fine particles is raised. In order to probe the effect of the fine particles on u_c' , it is necessary to compare the radial distribution of u_c' in the monodisperse system with that in the bidisperse systems for the same number of coarse particles. The addition of the fine particles affects the axial rms velocity of the coarse particles by increasing the magnitude of u_c' exceeding that in the monodisperse system and the enhancement of u_c' becomes more pronounced with increasing the radial distance. The higher magnitude of u_c' with the presence of the fine particles seems to agree with the proposed hypothesis of the increased apparent gas-phase viscosity. Since the presence of fine particles increases the gas-phase effective viscosity, the coarse particles experience a greater of resistance to move in the flow because they have to move both the fluid and fine particles. The increase in the resistance will make the motion of the coarse particles less random, hence reducing the frequency of the inter-particle collision for the coarse particles. Moreover, the large increase of u_c' near the pipe wall, observed in Fig. 25, is also possibly induced by the modification in the U_c profile observed in Fig. 24. Since the generation rate of u_c' via the fan spreading mechanism increases with increasing $\partial U_c / \partial r$, it is likely that the fan spreading mechanism is responsible for the greater magnitude of u_c' near the pipe wall.

Fig. 26 displays the radial distribution of the radial rms velocity for the 70-micron particles, v_c' , as a function of mass fraction of the fine particles. Unlike u_c' , the radial rms velocity, v_c' , shows a consistent decrease in magnitude as the mass fraction of the finer

particle increases. This trend is similar to that observed in monodisperse system with reducing the solid loading. The presence of the fine particles does not have a significant effect on v_c' . This concluded that the modulation in the magnitude of v_c' with varying mass fraction of the fine particles is mostly attributed to the variation on the number of the coarse particles, not due to the presence of the fine particles.

The effect of increasing mass fraction of the fine particles in the bidisperse system on the rms velocities of the fine particles, u_f' and v_f' , is displayed in Fig. 27. The magnitude of u_f' increases and v_f' decreases as the mass fraction of the fines is raised. The modification on the rms velocities of the fine particles in the bidisperse system is not attributed to the direct collision between the 25 and 70-micron particles, but rather due to the change in the number of the fine particles (solid loading of the fines) as observed in the monodispersed suspension results. In addition, Fig. 27, which compares the velocity fluctuations of the fine particles, u_f' and v_f' in the monodisperse system with those in the bidisperse system for the same number of the fine particles ($m=0.5$), shows no variation of u_f' and v_f' for the two suspensions. This observation suggested that the presence of the coarse particles does not affect the velocity fluctuations of the fine particles and the flow behavior of the fine particles in the bidisperse system is only a function of the number of the fine particles in the system, just like in the monodisperse system. Moreover, the similarities in the magnitudes of u_f' and v_f' for both systems are also attributed to the similarity in the level of gas turbulence in which the fine particles are exposed.

In summary, our LDV measurements indicate that the axial mean and rms velocities of the coarse particles (75 micron) are enhanced by the presence of the finer particles (25 micron). On the other hand, the motion of the finer particles was not influenced by the presence of the coarser particles.

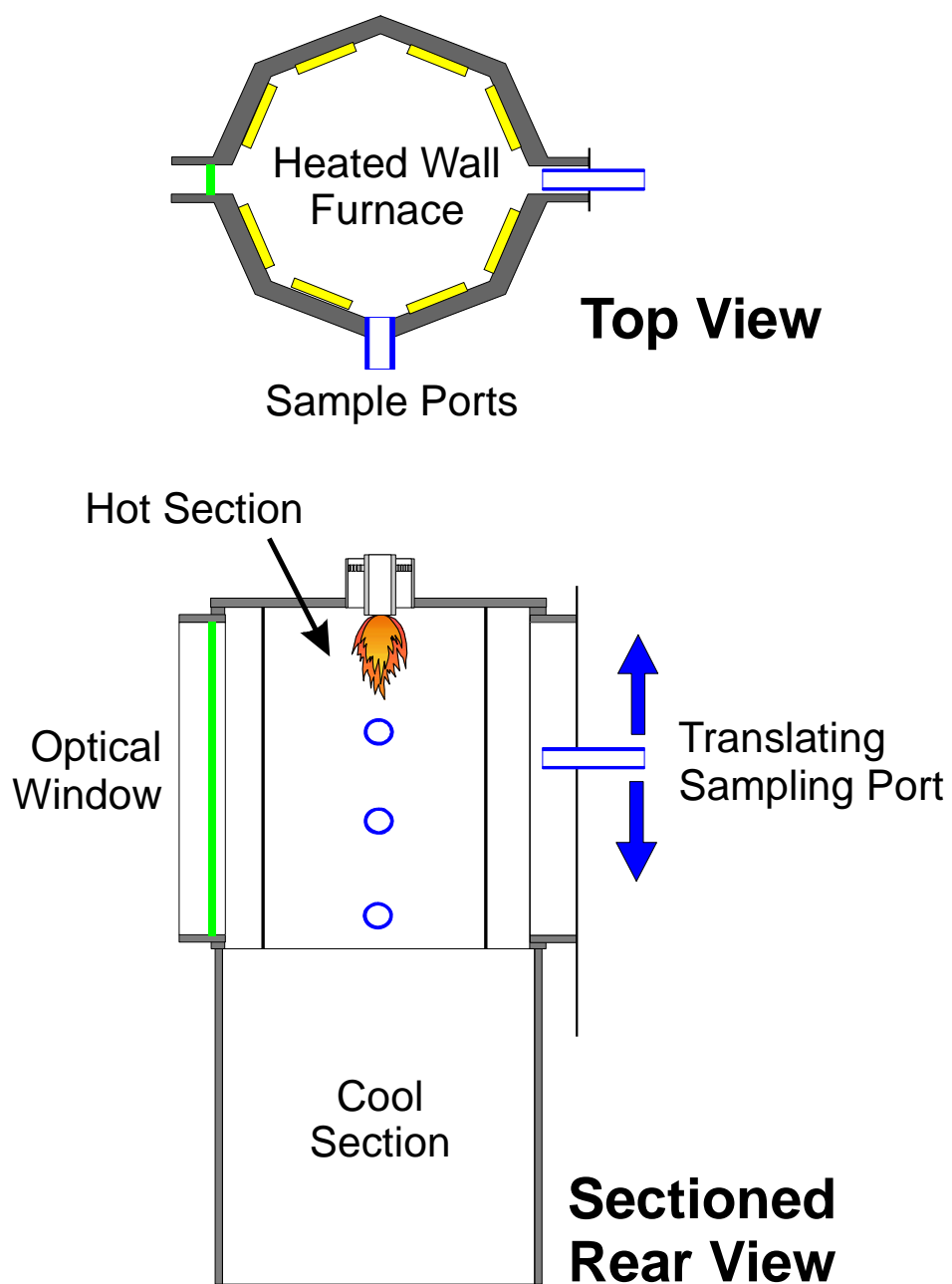
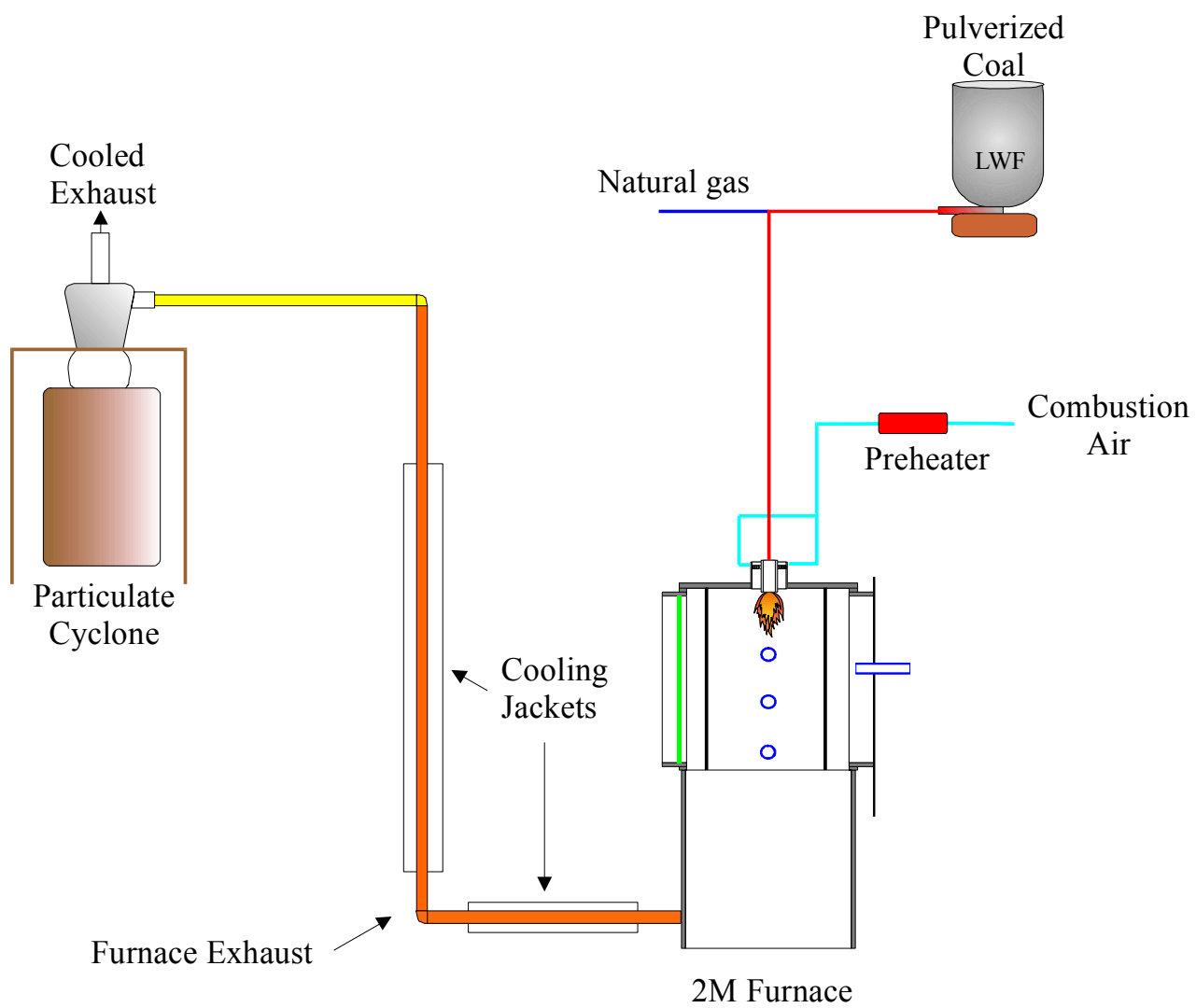


Figure 1. Schematic of 2M Furnace

Figure 2. Process Flow Diagram of Hot Flow System



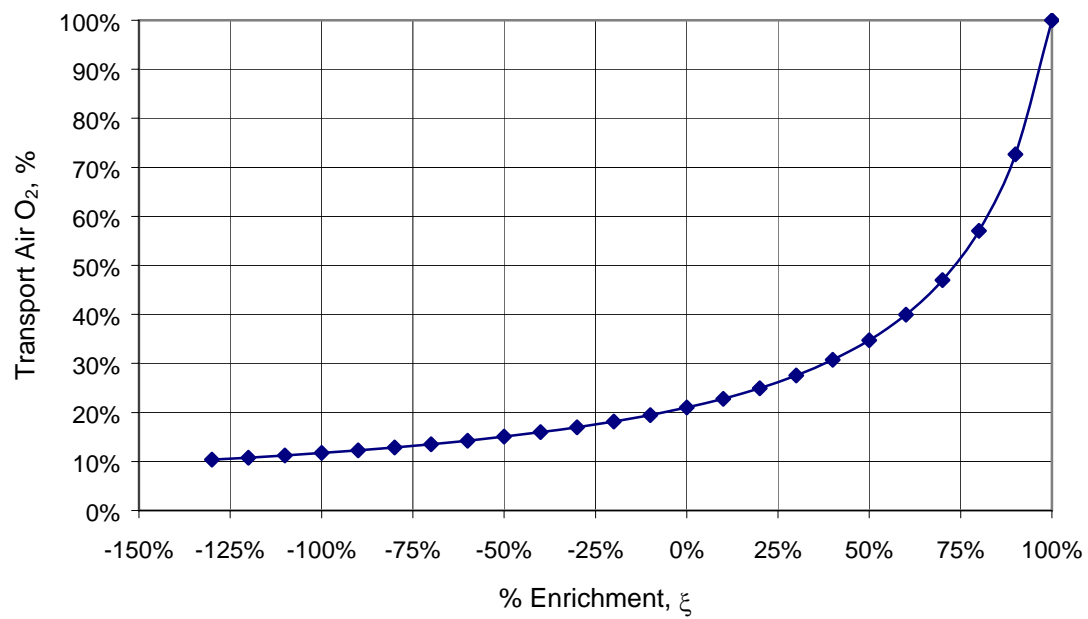
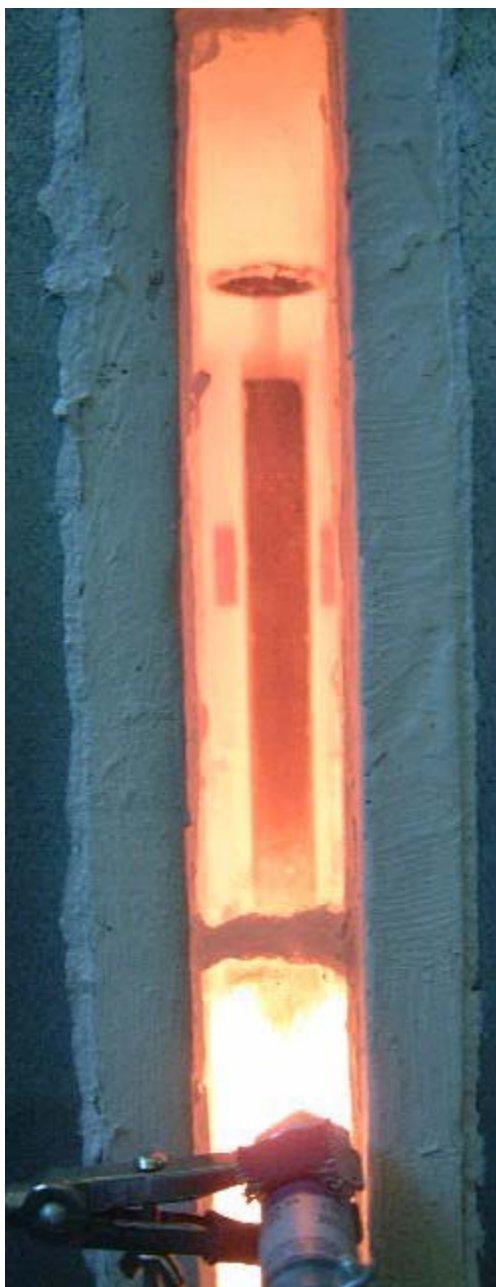


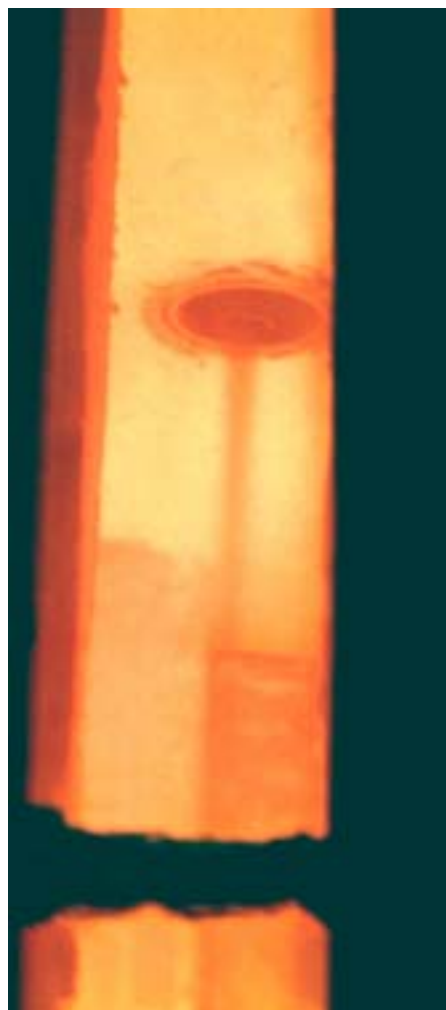
Figure 3. Effect of Oxygen Enrichment on Transport Air Oxygen



Figure 4. Stable Attached Coal Flame
17% Transport Air Oxygen, 900°C Walls



5a. Detached Flame,
Stabilized 15" below burner



5b. Coal Stream of Detached
Flame.

Figure 5. Stable Detached Flame

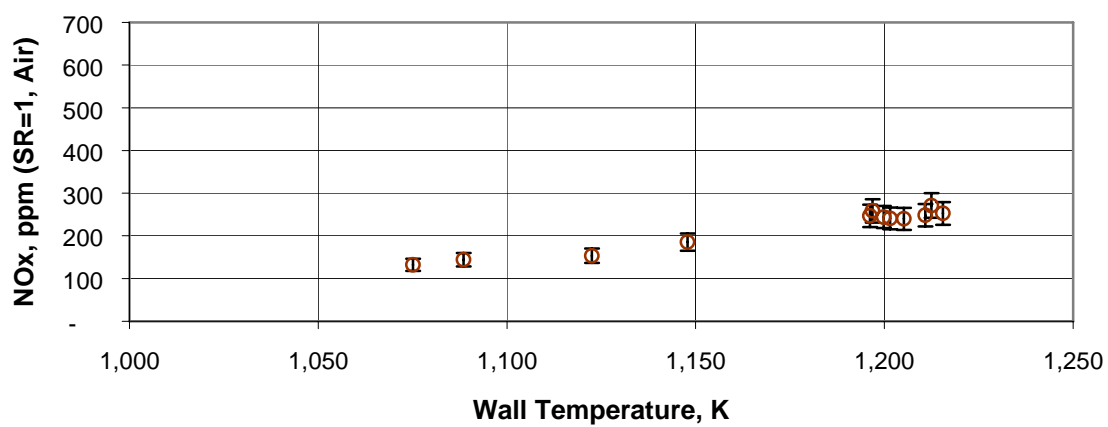


Figure 6. NO_{x,SR} vs. Temperature- 17% Transport Air O₂-Attached Flames

Open symbols are at a velocity ratio (VR) = 3.

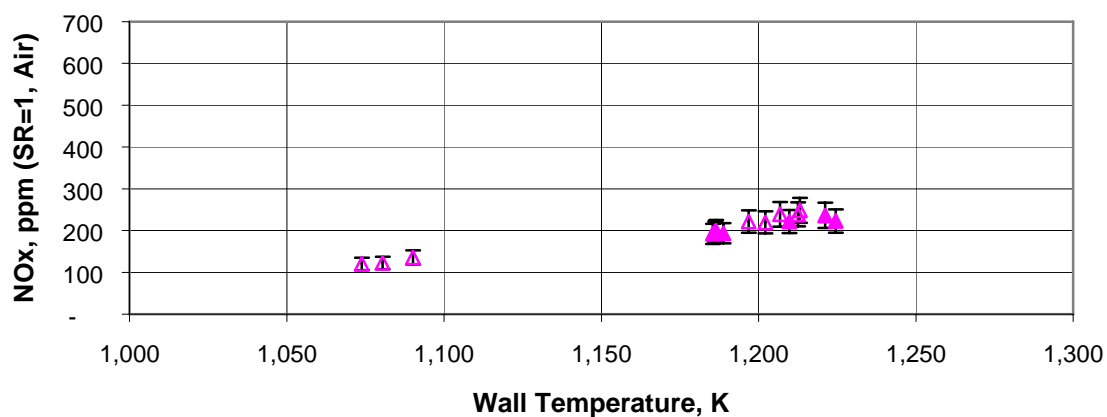


Figure 7. $\text{NO}_{x,\text{SR}}$ vs. Temperature- 21% Transport Air O_2 -Attached Flames

Open symbols are at VR = 3, Close symbols are at VR = 1.5

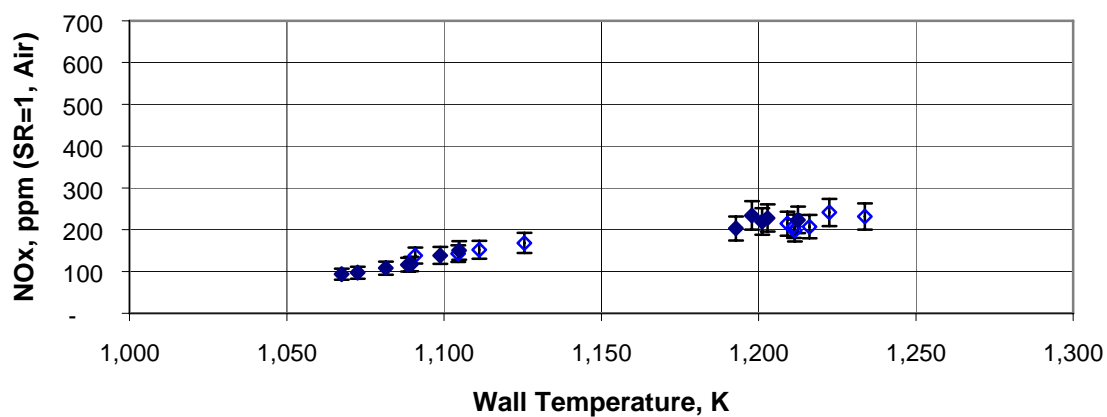


Figure 8. $\text{NO}_{x,\text{SR}}$ vs. Temperature- 24% Transport Air O_2 -Attached Flames

Open symbols are at VR = 3, Close symbols are at VR = 1.5

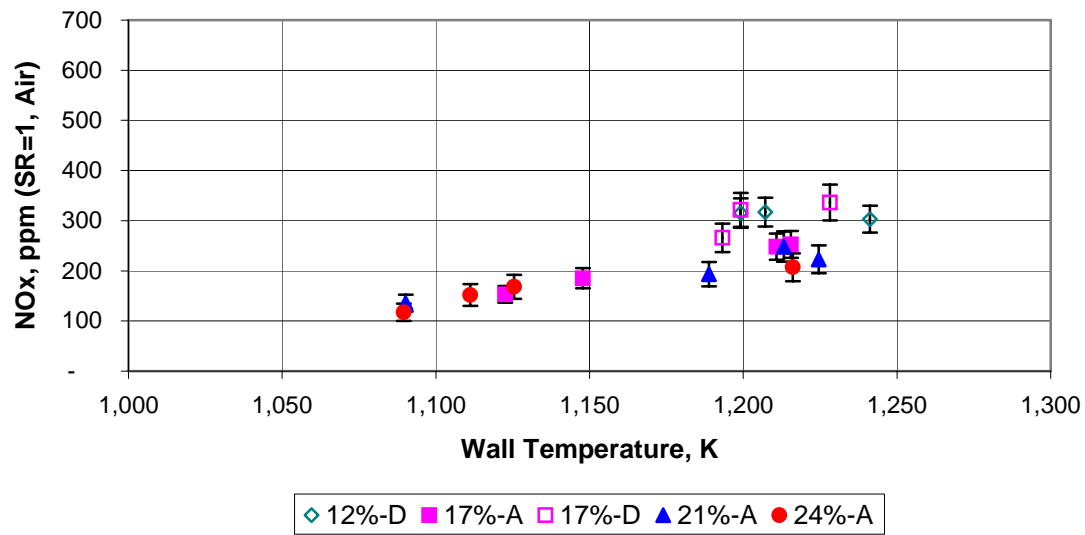


Figure 9. NO_{x,SR} vs. Temperature-Attached and Detached Flames

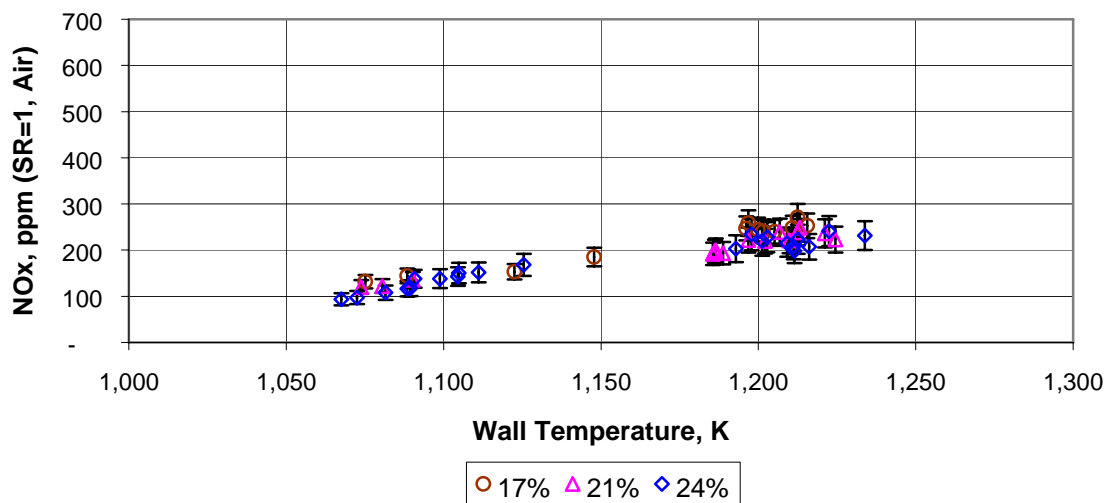


Figure 10. Combined NO_{x,SR} vs. Temperature-Attached Flames

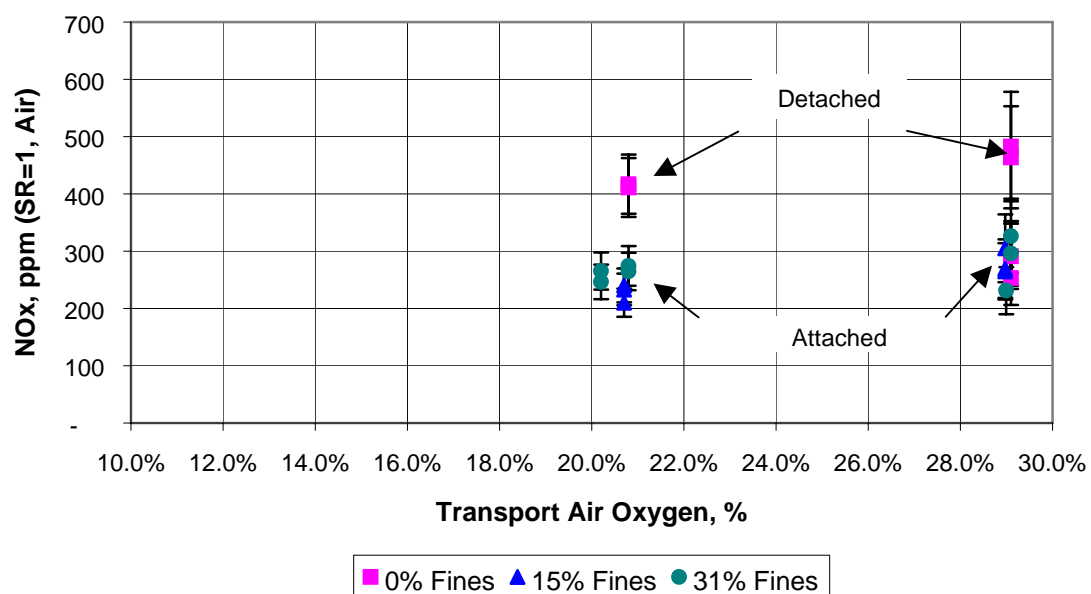


Figure 11. NO_{x,SR} vs. Transport Air Oxygen

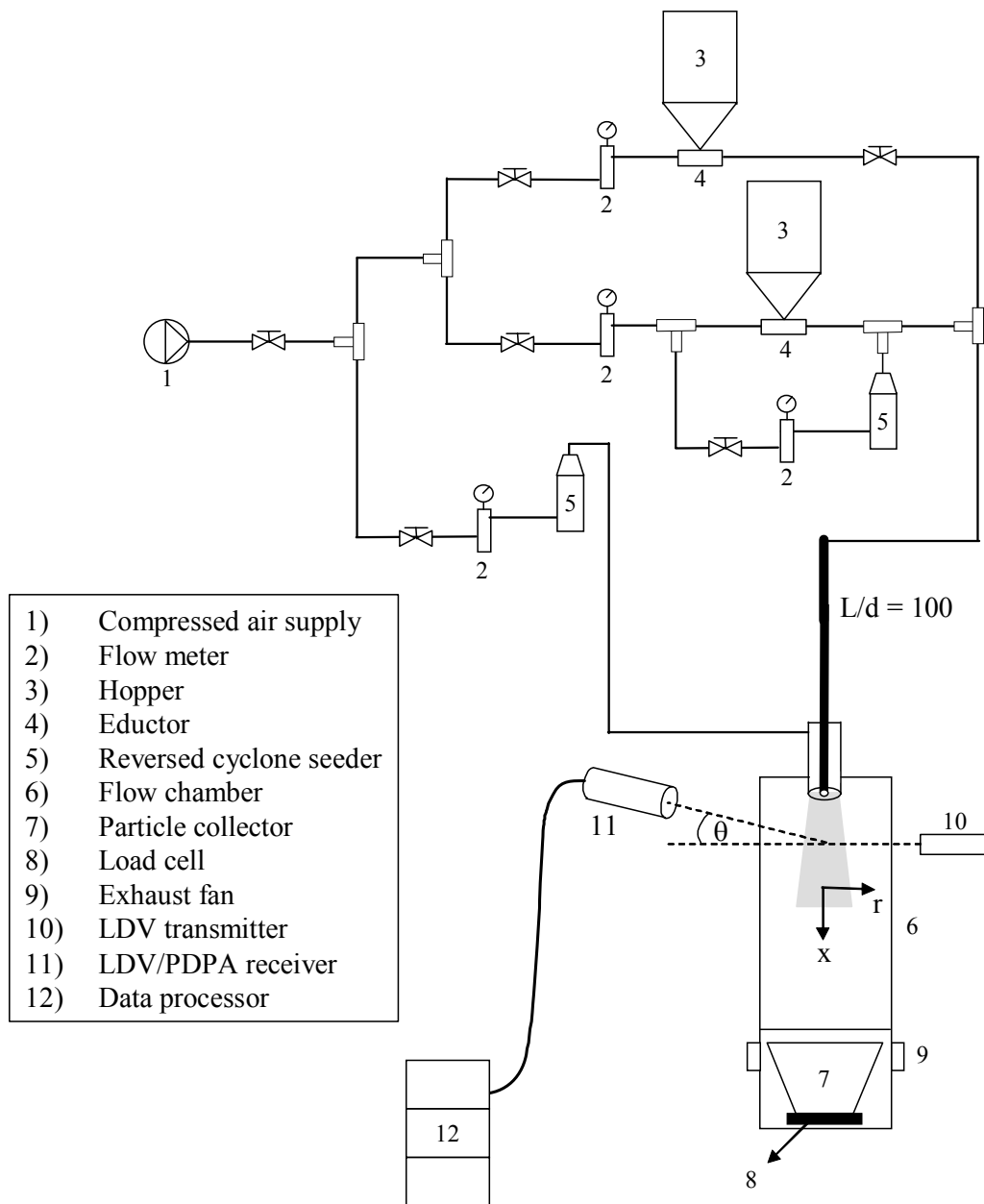
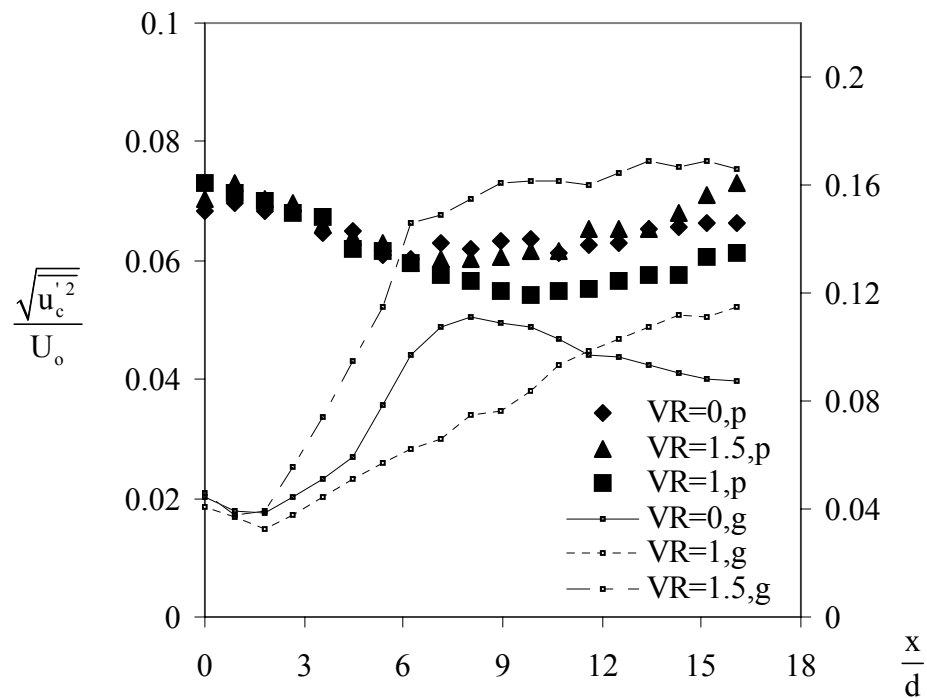


Figure 12. Schematic of LDV System

(a)



(b)

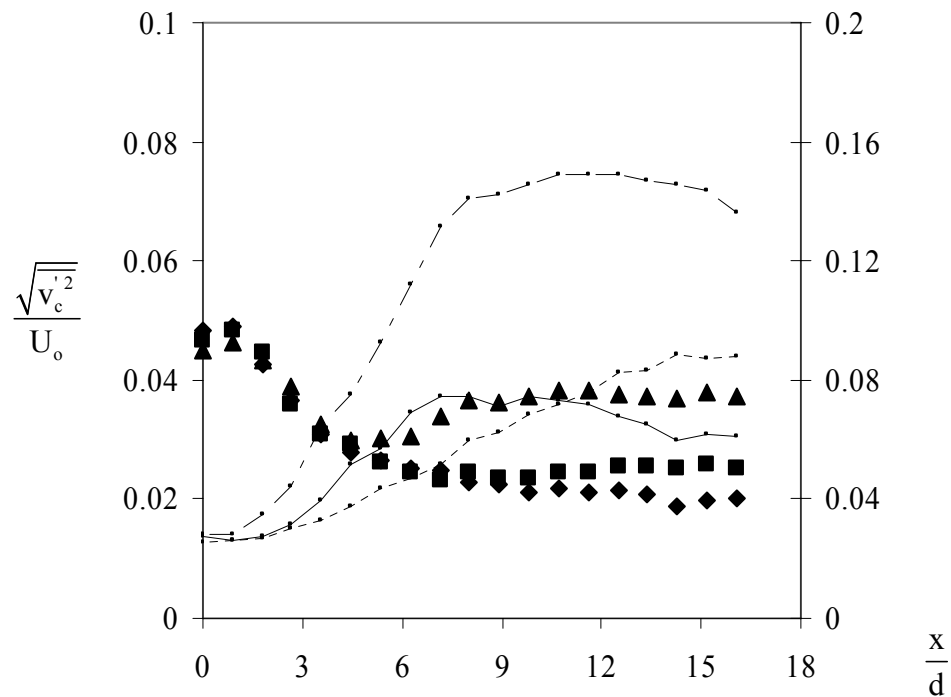
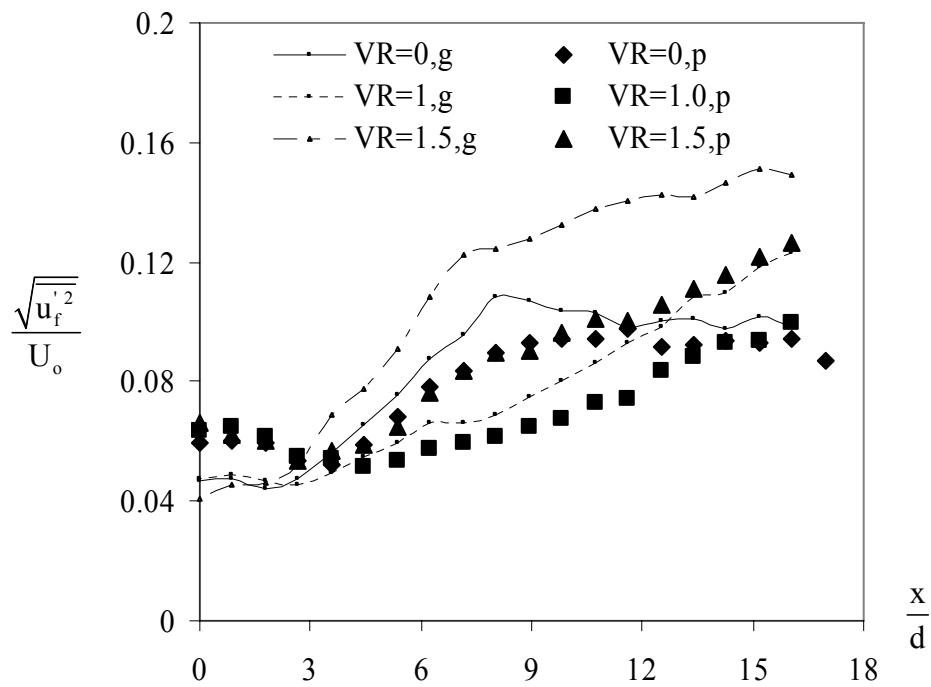


Figure 13. Effect of velocity ratio on the centerline development of (a) axial rms velocity and (b) radial rms velocity for the 70-micron particles.

(a)



(b)

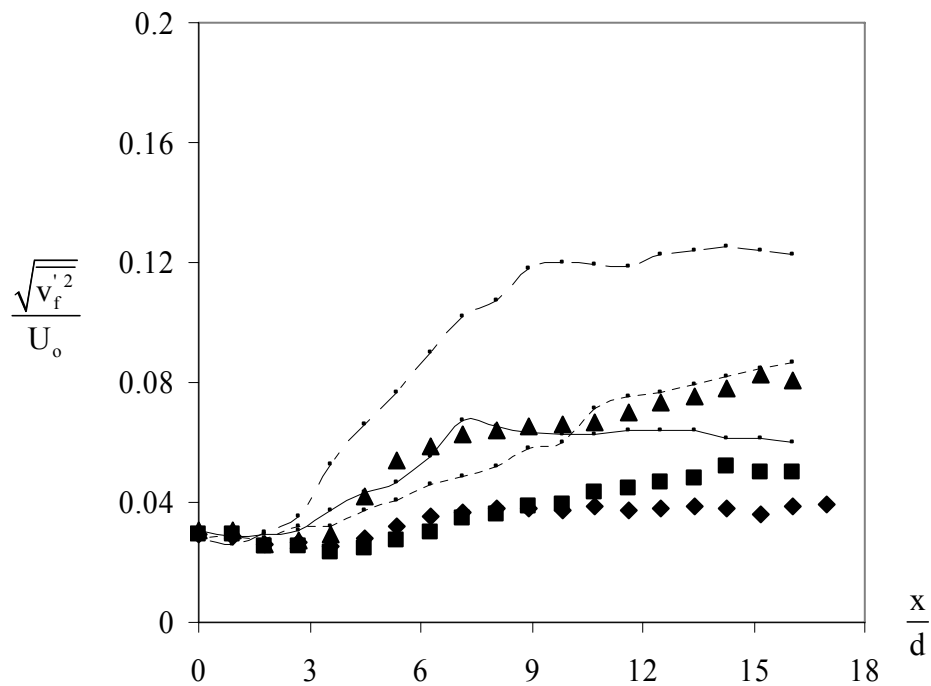


Figure 14. Effect of velocity ratio on the centerline development of (a) axial rms velocity and (b) radial rms velocity for the 25-micron particles.

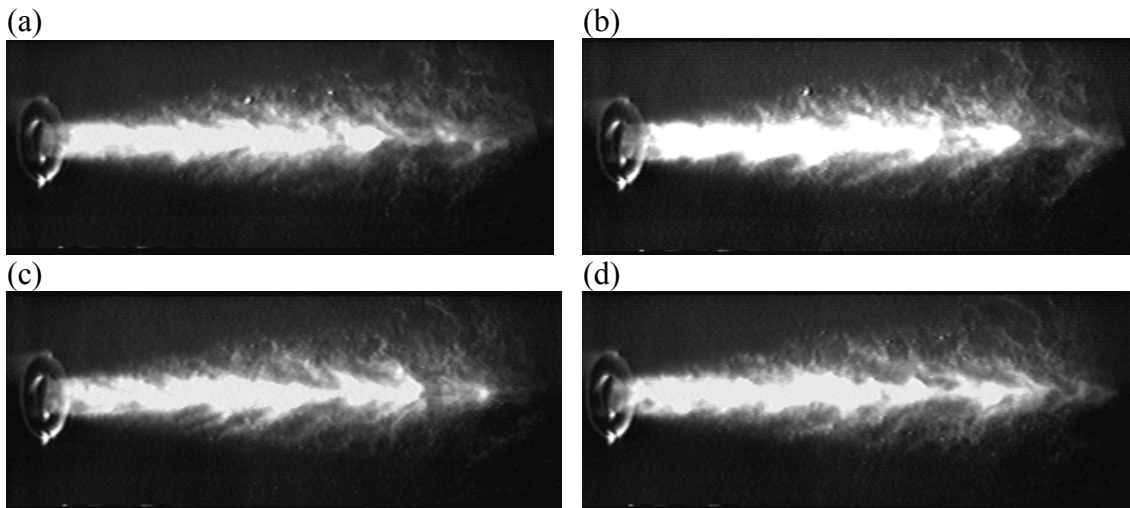


Figure 15. Sequence of photographic snapshots for the 25-micron particles in a coaxial jet with $VR = 0$ taken with a time interval 0.0025 second.

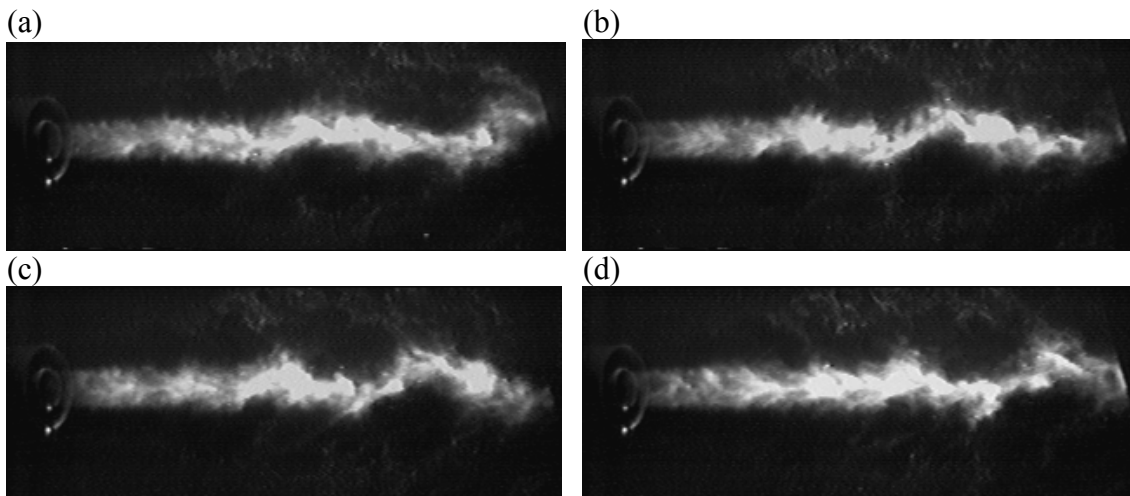


Figure 16. Sequence of photographic snapshots for the 25-micron particles in a coaxial jet with $VR = 1.0$ taken with a time interval 0.0025 second.

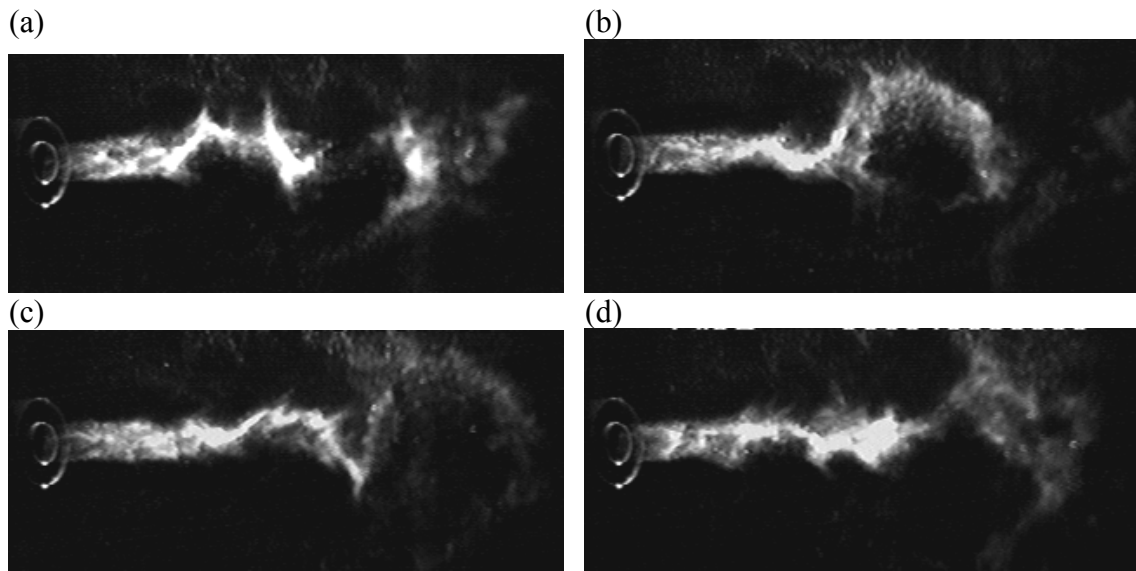


Figure 17. Sequence of photographic snapshots for the 25-micron particles in a coaxial jet with $VR = 1.5$ taken with a time interval 0.0041 second.

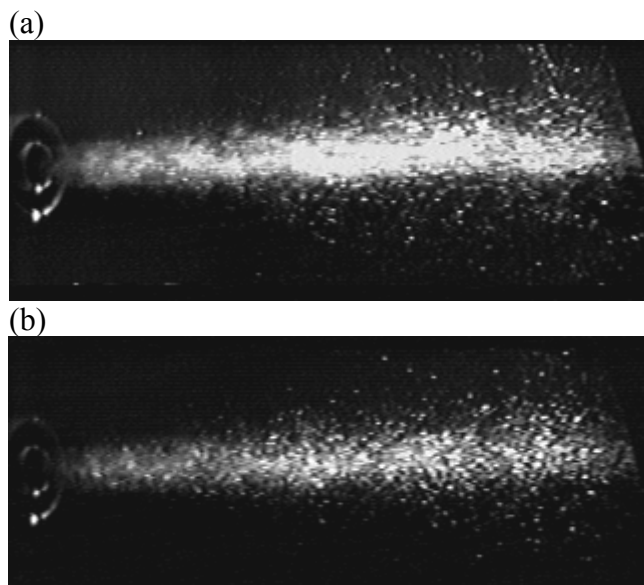


Figure 18. Photographic snapshots for the 70-micron particles in a round laden jet taken with shutter speed of (a) $1/2000$ s and (b) $1/4000$ second.

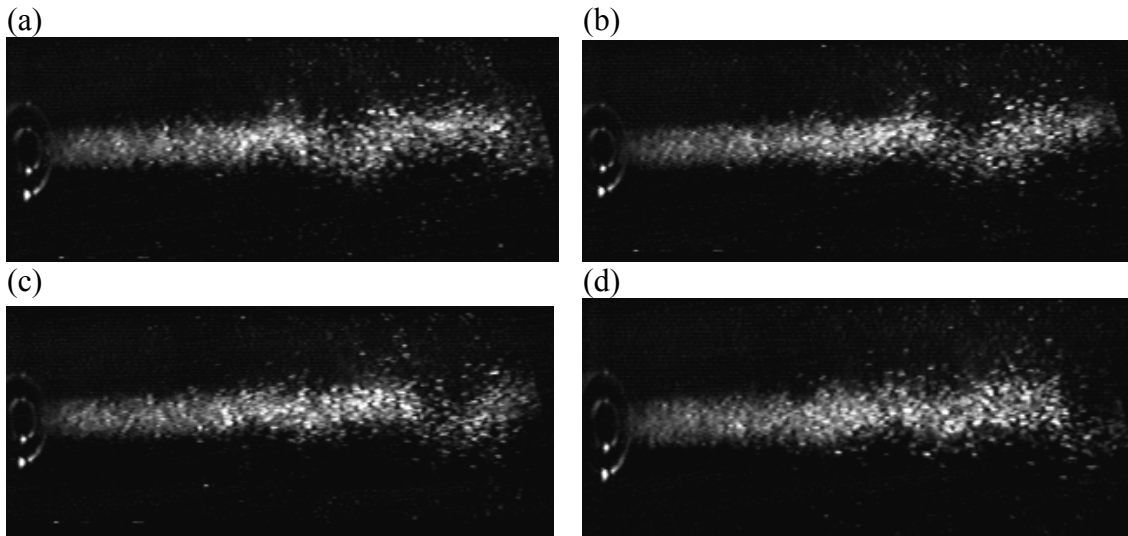


Figure 19. Sequence of photographic snapshots for the 70-micron particles in a coaxial jet with $VR = 1.0$ taken with a time interval 0.0025 second.

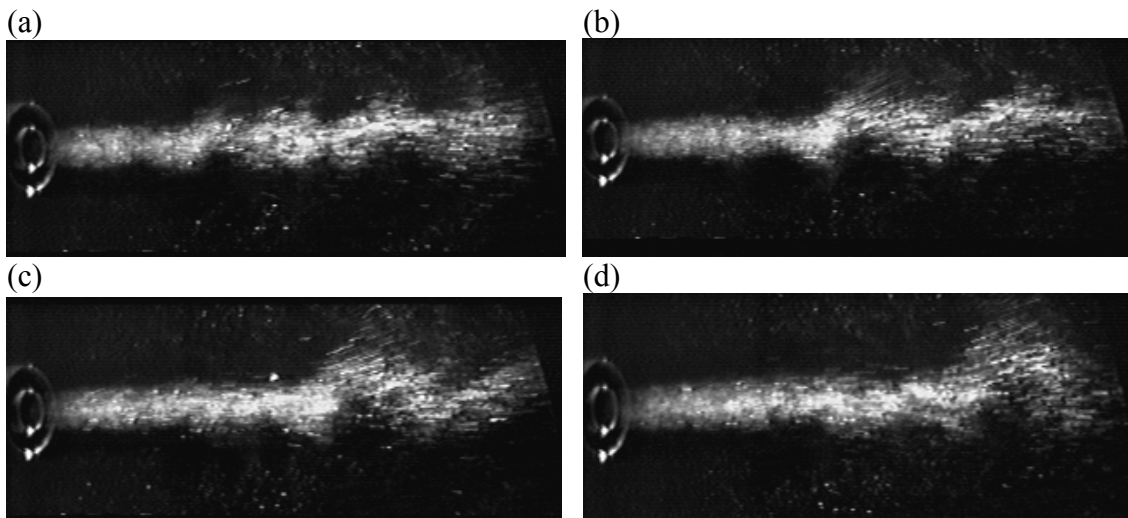


Figure 20. Sequence of photographic snapshots for the 70-micron particles in a coaxial jet with $VR = 1.5$ taken with a time interval 0.0025 second.

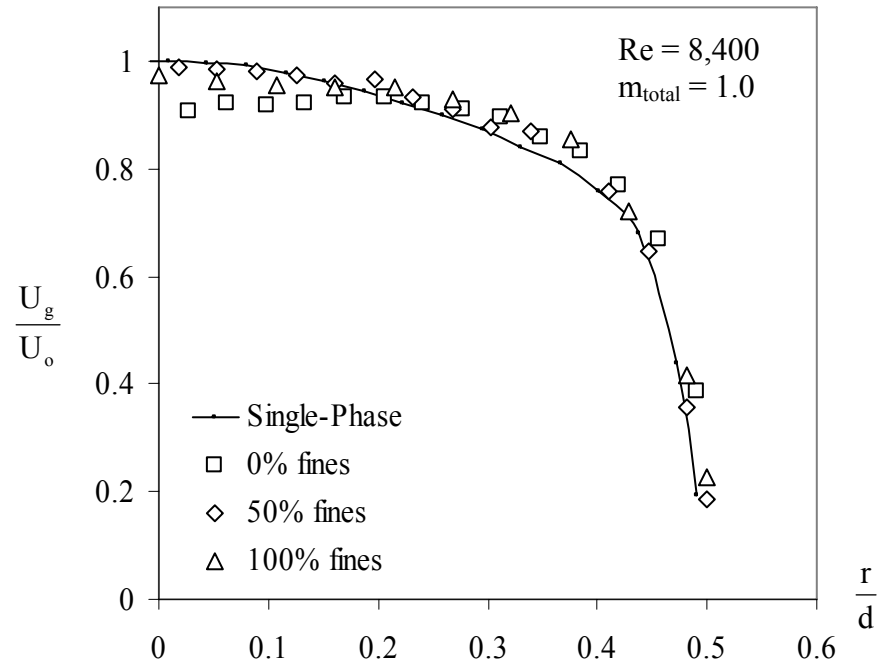
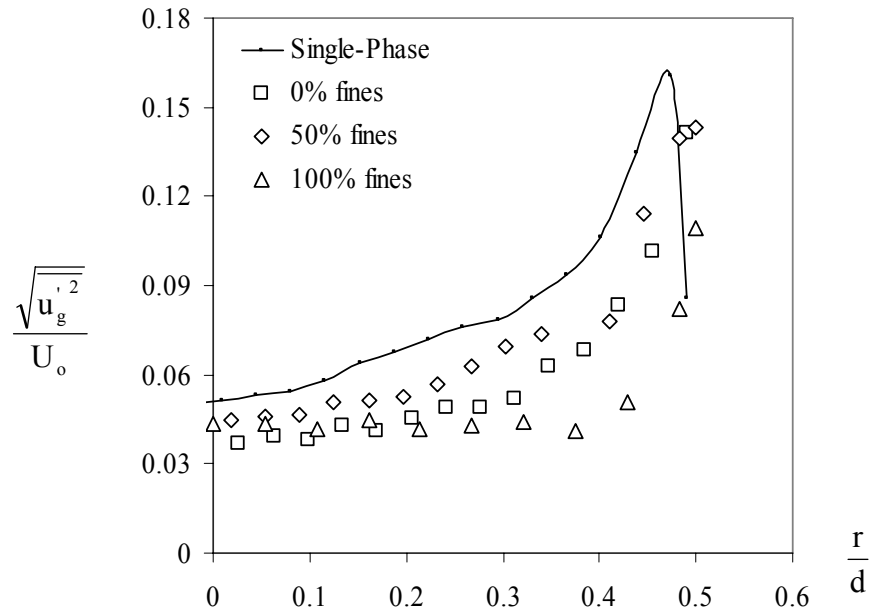


Fig. 21. Radial profiles of axial mean gas velocity, U_g , as a function of mass fraction of the fine particles in the bidisperse suspension.

(a)



(b)

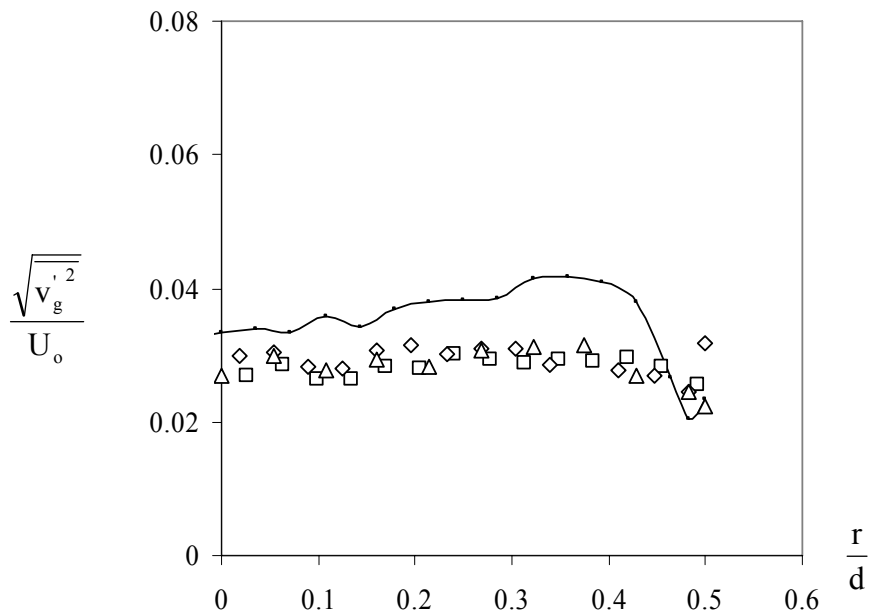


Fig. 22. Effect of varying mass fraction of the fine particles in the bidisperse suspension on (a) axial rms velocity and (b) radial rms velocity of the gas-phase.

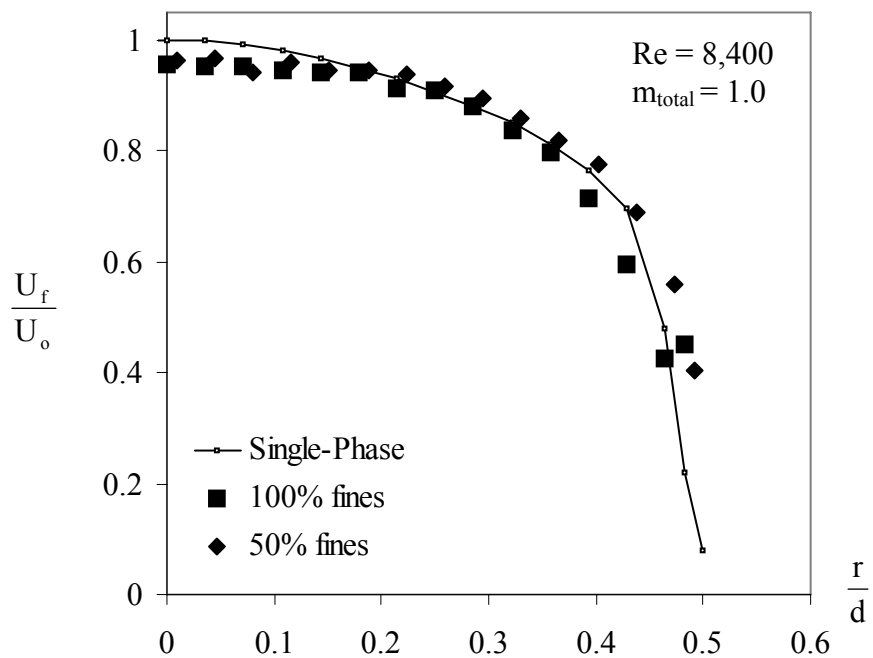


Fig. 23. Radial profiles of axial mean velocity of the 25-micron particles, U_f , as a function of mass fraction of the fine particles in the bidisperse suspension.

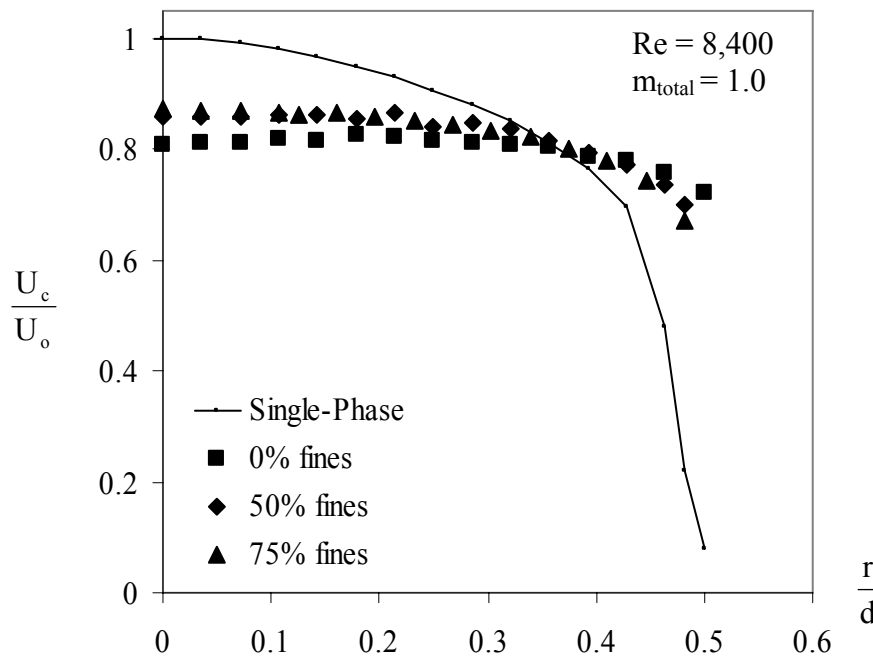


Fig. 24. Radial profiles of axial mean velocity of the 70-micron particles, U_c , as a function of mass fraction of the fine particles in the bidisperse suspension.

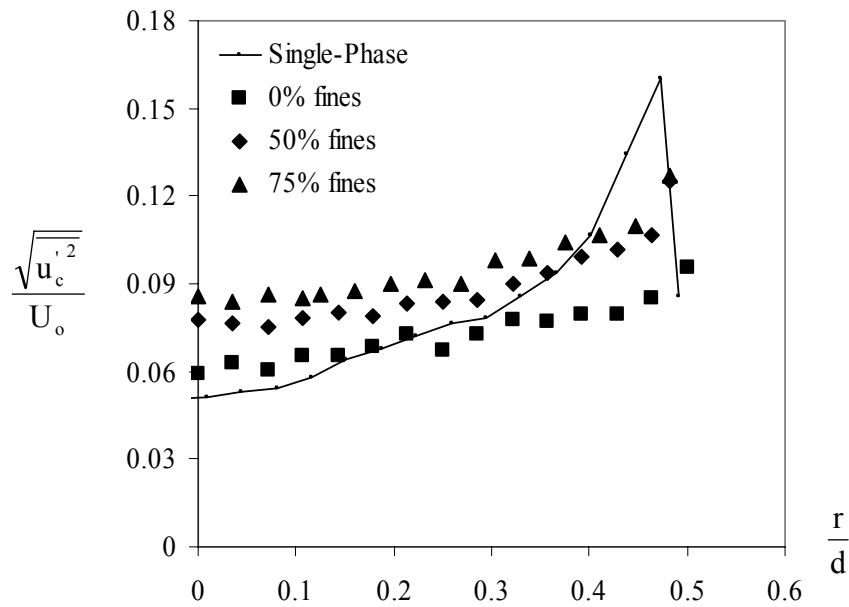


Fig. 25. Radial profiles of axial rms velocity of the 70-micron particles, u_c' , as a function of mass fraction of the fine particles (bidisperse suspensions) at the nozzle exit.

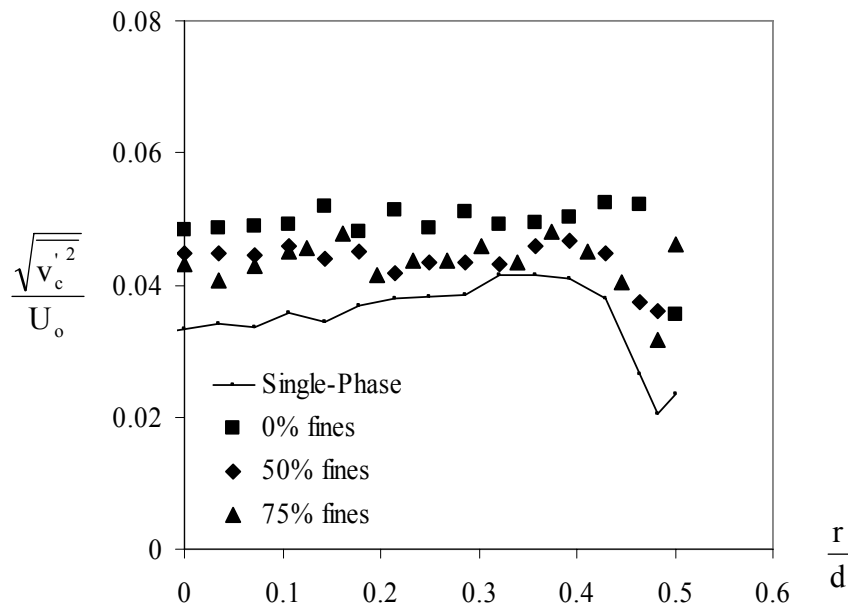
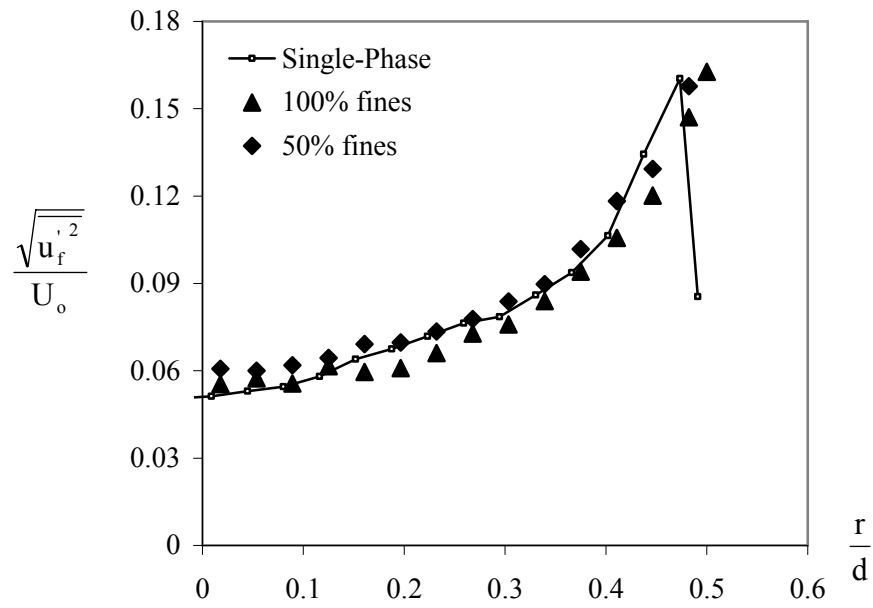


Fig. 26. Effect of varying mass fraction of the fine particles in the bidisperse suspension on the radial rms velocity of the 70-micron particles.

(a)



(b)

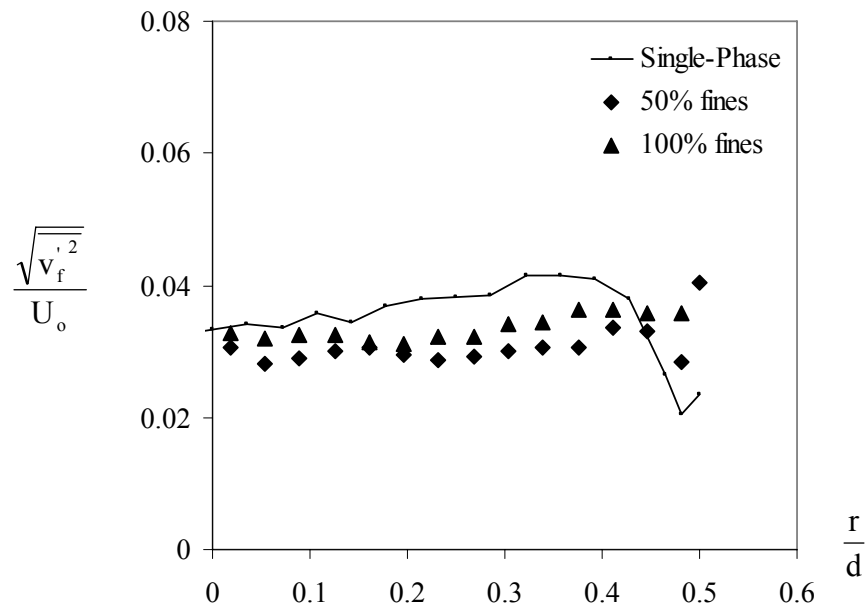


Fig. 27. Effect of varying mass fraction of the fine particles on (a) axial rms velocity, u_p' , and (b) radial rms velocity of the 25-micron particles

Table 1. Partial Pressure Experimental Matrix

run	SR	O ₂	Split	Ta %O ₂	Vc	Vt	Wall T	O ₂ pp	Notes
1	1.2	0%	10	21.0%	31.8	19.4	750	147	Unstable blew out at 5 minutes
2	1.2	15%	11.5	23.8%	31.2	19.6	750	167	Stable attached
3	1.2	-30%	8.1	17.0%	32.5	19.4	750	120	Unstable w/o gas
4	1.17	-100%	5.7	11.7%	32.5	19.3	750	82	Unstable w/o gas
5	1.2	0%	10	21.0%	31.8	19.4	900	147	Unstable w/o gas
6	1.2	15%	1.5	23.8%	31.2	19.6	900	167	Detached after a few minutes
7	1.2	-30%	8.1	17.0%	32.5	19.4	900	120	Immediately detached
8	1.17	-100%	5.7	11.7%	32.5	19.3	900	82	Immediately detached
9	1.2	0%	10	21.0%	31.8	11.6	750	147	Attached
10	1.2	15%	11.5	23.8%	31.2	11.8	750	167	Attached
11	1.2	-30%	8.7	17.0%	32.5	11.6	750	120	Attached
12	1.17	-100%	5.7	11.7%	32.5	11.6	750	82	Did not run
13	1.2	0%	10	21.0%	31.8	11.6	900	147	Attached
14	1.2	15%	11.5	23.8%	31.2	11.8	900	167	Attached
15	1.2	-30%	8.1	17.0%	32.5	11.6	900	120	Attached
16	1.17	-100%	5.7	11.7%	32.5	11.6	900	82	Immediately detached

References

- Baukal, C.E., **Oxygen-enhanced Combustion**, CRC Press, Boca Raton, FL, 1998.
- Becker, H.A., Hottel, H.C., Williams, G.C., "Mixing and Flow in Ducted Turbulent Jets", 9th International Symposium on Combustion, The Combustion Institute, 1963, pp.7-20.
- Pershing, D.W., Ph.D. Dissertation, University of Arizona, 1976.
- Smart, J.P., Ph.D. Dissertation, University of London, 1992.
- Spinti, J.P., Pershing, D.W., Brouwer, J., Heap, M.P., "Influence of Near Burner Combustion Modifications on NO_x formation from an All-Axial Multifuel Burner", *Combust Sci Technol.*, **126**(1), 1997, pp.1-6.
- Thring, M.W., Newby, M.P., "Combustion Length of Enclosed Turbulent Jet Flames", 4th International Symposium on Combustion, The Combustion Institute, 1952, pp.789-796.
- Yanta, W. and Smith, R., "Measurements of Turbulence-Transport Properties with a Laser Doppler Velocimetry," *AIAA 11th Aerospace Sciences Meeting, AIAA Paper No. 73-169*, Washington, D.C. (1973).

List of Journal Articles and Presentations:

Ogden, G.E., Budilarto, S.G., Sinclair, J.L., Wendt, J.O.L., "Comparison of Velocity vs. Momentum for Stabilizing Turbulent Natural Gas Flames" Presented at the 2000 Spring Meeting, AFRC, Newport Beach, CA, June 1-5, 2000.

Budilarto, S. G. and Sinclair, J.L., "Velocity Ratio Effect on Gas and Particle Motion in a Two-Phase Coaxial Jet", Presented at the 2000 Annual AIChE Meeting, Los Angeles, CA, November 2000.

Budilarto, S.G., and Sinclair, J.L., "Effect of Velocity Ratio on Co-axial Jet Flow Behavior", Presented at the International Conference on Multiphase Flow, New Orleans, LA, May 2001.

Budilarto, S.G., and Sinclair, J.L., "Effect of Particle Size on Particle Flow Patterns in Co-axial Jets", Presented at the 2001 Annual AIChE Meeting, Reno, NV, November 2001.

Budilarto, S.G., and Sinclair, J.L., "Flow Visualization of Particle-Laden Coaxial Jet Flow", Presented at the 2002 Annual AIChE Meeting, Indianapolis, IN, November 2002.

Budilarto, S.G. and Sinclair, J.L., "An Experimental Study on Effect of Particle Size Distribution in Particle-laden Jet Flows", 2003 Annual AIChE Meeting, San Francisco, CA, November 2003.

PhD Students Who Received Support from the Grant:

Greg Ogden, PhD Student, University of Arizona, Dept. of Chemical & Environmental Engineering

Steve Budilarto, PhD Student, Purdue University, School of Chemical Engineering